



Evaluation of predicted knee function for component malrotation in total knee arthroplasty

Vanheule, Valentine; Delpont, Hendrik Pieter; Andersen, Michael Skipper; Scheys, Lennart; Wirix-Speetjens, Roel; Jonkers, Ilse; Victor, Jan; Vander Sloten, Jos

Published in:
Medical Engineering & Physics

DOI (link to publication from Publisher):
[10.1016/j.medengphy.2016.12.001](https://doi.org/10.1016/j.medengphy.2016.12.001)

Publication date:
2017

Document Version
Accepted author manuscript, peer reviewed version

[Link to publication from Aalborg University](#)

Citation for published version (APA):
Vanheule, V., Delpont, H. P., Andersen, M. S., Scheys, L., Wirix-Speetjens, R., Jonkers, I., Victor, J., & Vander Sloten, J. (2017). Evaluation of predicted knee function for component malrotation in total knee arthroplasty. *Medical Engineering & Physics*, 40(1), 56-64. <https://doi.org/10.1016/j.medengphy.2016.12.001>

General rights

Copyright and moral rights for the publications made accessible in the public portal are retained by the authors and/or other copyright owners and it is a condition of accessing publications that users recognise and abide by the legal requirements associated with these rights.

- Users may download and print one copy of any publication from the public portal for the purpose of private study or research.
- You may not further distribute the material or use it for any profit-making activity or commercial gain
- You may freely distribute the URL identifying the publication in the public portal -

Take down policy

If you believe that this document breaches copyright please contact us at vbn@aub.aau.dk providing details, and we will remove access to the work immediately and investigate your claim.

1 **1. Title page**

2

3 **Evaluation of predicted knee function for**
4 **component malrotation in total knee**
5 **arthroplasty**

6

7 Valentine Vanheule^{a,b}, Hendrik Pieter Delpoort^c, Michael Skipper Andersen^d, Lennart Scheys^c,
8 Roel Wirix-Speetjens^b, Ilse Jonkers^e, Jan Victor^f and Jos Vander Sloten^a

9

10 ^aBiomechanics section, Katholieke Universiteit Leuven, Celestijnenlaan 300C, 3001 Leuven, Belgium

11 ^bMaterialise N.V., Technologielaan 15, 3001 Leuven, Belgium

12 ^cDepartment of Orthopaedics, University Hospital Pellenberg, Katholieke Universiteit Leuven, Weligerveld 1, 3212
13 Pellenberg, Belgium

14 ^dDepartment of Mechanical and Manufacturing Engineering, Aalborg University, Fredrik Bajers Vej 5, 9100 Aalborg,
15 Denmark

16 ^eDepartment of Kinesiology, Katholieke Universiteit Leuven, Tervuursevest 101, 3001 Leuven, Belgium

17 ^fDepartment of Physical Medicine and Orthopedic Surgery, Ghent University, De Pintelaan 185, 9000 Ghent, Belgium

18

19

20

21

22

23

24

25

26 **Corresponding author**

27 Valentine Vanheule

28

29 Department of Mechanical Engineering

30 Division BMe

31 Celestijnenlaan 300C

32 3001 Leuven, Belgium

33 valentine.vanheule@kuleuven.be

34 Phone: +32 16 74 42 71

35 Fax: +32 16 39 66 00

36

37 **2. Abstract**

38 Soft-tissue balancing for total knee arthroplasty (TKA) remains subjective and highly
39 dependent on surgical expertise. Pre-operative planning may support the clinician in taking
40 decisions by integrating subject-specific computer models that predict functional outcome.
41 However, validation of these models is essential before they can be applied in clinical practice.
42 The aim of this study was to evaluate a knee modelling workflow by comparing experimental
43 cadaveric measures to model-based kinematics and ligament length changes. Subject-specific
44 models for three cadaveric knees were constructed from medical images. The implanted knees
45 were mounted onto a mechanical rig to perform squatting, measuring kinematics and ligament
46 length changes with optical markers and extensometers. Coronal malrotation was introduced
47 using tibial inserts with a built-in slope. The model output agreed well with the experiment in
48 all alignment conditions. Kinematic behaviour showed an average RMSE of less than 2.7 mm
49 and 2.3° for translations and rotations. The average RMSE was below 2.5% for all ligaments.
50 These results show that the presented model can quantitatively predict subject-specific knee
51 behaviour following TKA, allowing evaluation of implant alignment in terms of kinematics and
52 ligament length changes. In future work, the model will be used to evaluate subject-specific
53 implant position based on ligament behaviour.

54 **Keywords:** subject-specific, alignment, soft tissue balancing, kinematic knee rig, in vitro

55

56

57

58

59

60

61 **3. Introduction**

62 Creating appropriate soft-tissue balance during total knee replacement surgery is mainly
63 subjective and highly dependent on the surgeon's expertise [1,2]. Pre-operative planning
64 incorporating predictive tools to evaluate functional outcome may support the surgeon by
65 comparing different surgical treatments. Subject-specific musculoskeletal models have a high
66 potential to be used as a predictive tool in clinical practice [3]. In detailed joint models,
67 ligaments strongly influence kinematics since they are highly important structures for guiding
68 and stabilising knee motion [4,5]. However, before applying such models in a clinical setting,
69 validation is of paramount importance. The purpose of this study was to evaluate a
70 computational efficient model that can predict subject-specific knee kinematics and ligament
71 length changes for different implant alignments.

72 Recently, several studies explored methods that can simultaneously compute motions as well
73 as muscle and contact forces. Hast and Piazza presented a dual-joint workflow in which the
74 knee joint is alternated between a simplified knee joint representation for inverse dynamics and
75 an unconstrained knee with elastic foundation contact [6]. Thelen et al. extended the computed
76 muscle control algorithm (CMC) to co-simulate muscle and contact forces, using an elastic
77 foundation model [7]. Guess et al. presented a two-stage modelling method, an inverse
78 kinematics and a forward dynamics simulation, predicting muscle and contact forces
79 concurrently [8].

80 Andersen et al. introduced an alternative approach, called force-dependent kinematics (FDK),
81 that extends the fast inverse dynamic simulations with the ability to estimate secondary joint
82 kinematics [9]. This method relies on an assumption of quasi-static force equilibrium in the
83 secondary joint kinematics at each time step during the analysis. In 2014, the FDK method was
84 applied and knee contact forces were validated during walking activities in the winning model
85 of the Grand Challenge competition [10].

86 Musculoskeletal models have the ability to explore the relationship between implant alignment
87 and functional outcome for different activities of daily living. Others investigated the effects of
88 implant alignment variation during a simulated squat, however, without collecting experimental
89 evidence for the malaligned configurations [11,12]. In our study, we modelled different implant
90 alignment variations and additionally, performed a cadaveric study to validate the predicted
91 knee function for each alignment. FDK was used to simulate knee kinematics and predict
92 ligament length change patterns for three cadaveric knees with TKA performing a squat motion.
93 In addition to the standard implant, malrotation in the coronal plane was introduced by using
94 tibial inserts with a built-in varus or valgus offset [13]. For each specimen, three squats were
95 performed with the knee in neutral, varus or valgus alignment. The model outputs were
96 validated by comparing experimental and model-predicted tibio-femoral motion and ligament
97 length changes. To our knowledge, this is the first study to both simulate and validate the impact
98 of implant alignment on kinematics and ligament length changes as predicted by computer
99 models.

100 **4. Methods**

101 **4.1. Experimental data collection**

102 **4.1.1. Specimen preparation and imaging**

103 Three cadaveric knee specimens were used for squat simulations in a dynamic knee simulator
104 system. The methodology of the specimen preparation was similar to the workflow described
105 by Victor et al. [14]. The study protocol was approved by the local Ethics Committee.

106 After thawing the fresh frozen specimens, full leg T1-weighted opposed-phase spoiled gradient
107 echo magnetic resonance imaging (MRI) scans were obtained using a 3T scanner (Ingenia,
108 Philips Healthcare) to visualise soft tissues. The slice thickness was 2 mm and all slices had an
109 in plane resolution of 0.9 mm x 0.9 mm. Subsequently, frames (Medtronic, MN, USA) with

110 reflective spherical markers were rigidly attached to femur, tibia and patella. Each frame carried
111 4 markers, which were 6 mm in diameter. The femoral frame was inserted within 21 cm from
112 the joint line, the tibial frame within 18 cm from the joint line and the patellar frame was inserted
113 onto the patella. To allow accurate three-dimensional motion tracking, a six-camera motion
114 capture system (Vicon MX40, Oxford, UK) was used. The optical markers could accurately be
115 located on the pre-operative and post-operative computed tomography (CT) scans.

116 Volumetric CT scans of the full lower leg with the attached markers were obtained on a dual-
117 source multidetector CT scanner (SOMATOM Definition Flash, Siemens), equipped with two
118 64-detector row units, using a slice thickness of 0.75 mm and a pitch of 0.8 mm/rev. The images
119 were processed in Mimics v. 17.0 (Materialise, Leuven, Belgium) to construct the bone models
120 of femur, tibia and patella. These bone geometries were used to identify bony landmarks.

121 Next, the hip and foot were removed from the full leg, with a femoral cut 32 cm proximal of
122 the joint line and a tibial cut 28 cm distal from the joint line. The quadriceps muscle was
123 dissected and its preserved tendon was fixed into a clamp. In addition, the semitendinosus
124 together with the semimembranosus muscle, as well as the biceps femoris muscle were
125 dissected and suture wires were attached to the preserved tendons. The proximal femur and
126 distal tibia were then embedded in aluminium containers, preserving the physiologic alignment
127 in the coronal plane and parallel with the container in the sagittal plane.

128 Two extensometers (MTS, Eden Prairie, MN, USA) were sutured to the medial and lateral
129 collateral ligaments by an experienced surgeon. The fixation of the extensometers was centred
130 over the joint line, on an unloaded and fully extended knee [15]. During the measurements,
131 ligament length change relative to the extended knee was calculated using the formula $\varepsilon = (L -$
132 $L_r)/L_r$, where L was the instantaneous length of the extensometer arms connected to the
133 ligament and L_r was the reference length at full extension.

134 **4.1.2. Total knee replacement and imaging**

135 An experienced surgeon (HD) performed the total knee arthroplasty on each specimen using a
136 posterior-stabilised total knee arthroplasty (Performance, Biomet Inc., Warsaw, IN, USA). In
137 addition to the tibial implant placed with standard alignment instrumentation, two variations of
138 the tibial insert were designed through additive manufacturing. These variations were able to
139 artificially simulate a TKA coronal malalignment by their built-in varus or valgus design. The
140 inserts were modelled so that the central height was preserved while making one side thicker
141 and the other side thinner than the neutral insert. For each specimen, three squat trials were
142 performed. Specimen 1 underwent squats with neutral insert, 5° varus insert and 5° valgus
143 insert. Specimen 2 and 3 underwent squats with neutral insert, 3° varus insert and 3° valgus
144 insert. The tibial insert thickness for specimen 2 and 3 was smaller, leading to a smaller varus
145 and valgus angle due to design limitations. The valgus insert squat of specimen 3 is not shown
146 in the results since the quadriceps ruptured during the last experiment.

147 After the trials, post-operative CT scans were made with the optical markers still attached on
148 the same scanner as the pre-operative scans, allowing to accurately document the implant
149 position.

150 **4.1.3. Knee simulator set-up**

151 The specimens were mounted onto a dynamic knee simulator system, based on the Oxford rig
152 [16]. This mechanical system permits six degrees-of-freedom (DOFs) for both the tibio-femoral
153 and the patello-femoral joint. The femoral container was connected to an artificial hip assembly
154 and the tibial container to an artificial ankle assembly. The quadriceps clamp was connected to
155 an actuator that could apply a variable quadriceps load. Both hamstring wires were connected
156 with constant-force springs of each 50 N (Type KKF 8077, Lesjöfors, Karlstad, Sweden). The
157 hip assembly could slide vertically and flex and extend, the ankle assembly allowed rotation in

158 all three directions and translated medio-laterally. Sensors detected the quadriceps force, ankle
159 force and relative hip height and these real-time data were processed in a closed feedback
160 system (LabVIEW, National Instruments, Texas, USA), allowing the performance of a squat
161 motion by moving the hip assembly and applying a variable quadriceps force to induce a
162 vertical ankle force of 111 N. The quadriceps load increased during knee flexion, starting from
163 a few hundred Newton at the beginning of the experiment and the load could go up to 2000 N
164 at deep knee bend. A full squat motion began around 30-40° knee flexion and went up to 110-
165 120°. The squat did not begin at full extension to prevent hyperextension [14].

166 Six infrared emitting cameras (MX40, Vicon, Oxford, UK) tracked the reflecting light from the
167 rigidly attached optical markers on femur, tibia and patella at a sampling frequency of 100 Hz.
168 This provided us an accurate measurement of the knee joint motion during squat. Throughout
169 knee flexion, the three-dimensional (3D) coordinates of the passive markers were tracked and
170 the relative position of all the important landmarks on femur and tibia were computed. The
171 distance between the ligament insertion points on femur and tibia or fibula was used as the
172 ligament length at any given position in the flexion arc of the knee joint.

173 **4.2. Computational model definition**

174 **4.2.1. Subject-specific knee model set-up**

175 The experimental set-up was implemented into the AnyBody Modeling System 6.0.5 (AnyBody
176 Technology A/S, Denmark). The knee model consisted of the subject-specific bone geometry
177 segmented from CT scans in Mimics 17.0 (Materialise N.V., Leuven, Belgium). The implant
178 position was determined by the post-operative CT scans. The contact between femoral and tibial
179 implant and between femoral implant and patella was modelled using a rigid-rigid STL-based
180 contact model. The contact forces were computed based on the penetration depth, d_i , of a vertex

181 into the opponent surface. The penetration volume V_i was approximated by the multiplication
182 of the penetration depth and the opponent triangle area A_i , so that for the i th vertex

$$V_i = A_i d_i \quad (1)$$

183 The direction of the contact force was determined by the normal of the triangle and the contact
184 force magnitude for each contributing element was computed using a linear force law between
185 the penetration volume and the pressure module P

$$F_i = PV_i \quad (2)$$

186 A pressure module of 4.6 GN/m^3 was used, based on previous tests where the trade-off between
187 the penetration depth and the numerical issues of solving contact between two surfaces with
188 high stiffness was investigated [10].

189 Four ligaments were defined: proximal and distal part of the medial collateral ligament (MCL),
190 lateral collateral ligament (LCL), medial patello-femoral ligament (MPFL) and lateral
191 epicondylo-patellar ligament (LEPL). The insertions were estimated based on an anatomical
192 atlas using the specimen's bony landmarks and two insertion sites of the MCL proximally and
193 distally on the tibia were identified (MCLprox and MCLdist) [14]. Ligaments were represented
194 as non-linear line segments that wrap over analytical surfaces approximating the relevant
195 geometries. One cylinder was placed medially on the tibia to allow the MCLdist to wrap around
196 the medial tibial condyle and another cylinder was fitted to the femoral implant to prevent the
197 quadriceps muscle from penetrating the implant during deep flexion. Two ellipsoids were
198 introduced to wrap the MPFL and LEPL around the femoral condyles (Figure 1).

199 Ligament force was modelled with the following force-displacement relationship [17]

$$f = \begin{cases} 1/4k\varepsilon^2/\varepsilon_l & 0 \leq \varepsilon \leq 2\varepsilon_l \\ k(\varepsilon - \varepsilon_l) & \varepsilon > 2\varepsilon_l \\ 0 & \varepsilon < 0 \end{cases} \quad (3)$$

200 where f is the tensile force, k the ligament stiffness, ϵ_l the linear strain limit set at 0.03 [18]
201 and ϵ the strain calculated with the ligament length L and its zero-load length L_0 using the
202 equation $\epsilon = (L - L_0)/L_0$. The zero-load length L_0 was computed using the following
203 definition:

$$L_0 = L_r / (\epsilon_r + 1) \quad (4)$$

204 in which L_r is the ligament reference length and ϵ_r the reference strain. The stiffness and
205 reference strain of MCL and LCL were based upon values given by Blankevoort and Huijkes
206 and can be found in Table 1 [17]. The ligament reference lengths were computed with the intact
207 knee in full extension. Not much information is available regarding the stiffness and reference
208 strain of the patellar ligaments MPFL and LEPL. The MPFL is the primary restraint to lateral
209 patellar displacement and lateral soft-tissues contribute less to the overall stability [19].
210 Accordingly, MPFL stiffness was chosen in the same range of MCL and LCL and lower values
211 were attributed to LEPL. Since patellar ligaments are tightest in full extension and slacken with
212 flexion, positive reference strain values were assigned in the same range of MCL and LCL [19].
213 Both MPFL and LEPL were represented by three line segments and their parameter values are
214 shown in Table 1.

215 To compare the model output to the local extensometer length changes, the reported model
216 ligament length changes were calculated using the formula $\epsilon_{model} = (L - L_r)/L_r$. Additional
217 to the extensometer length changes, kinematic based ligament length changes were measured
218 by tracking the length changes of the ligament line segment during the experimental motion
219 compared to the length at full extension.

220 The simulation mimicked the experimental set-up, such that the same force to the quadriceps
221 tendon was applied and the same vertical motion of the hip assembly was generated. Figure 2
222 shows how the model was constrained during the simulation. The hip assembly could move up

223 and down and flex and extend. The ankle assembly could rotate in all three directions and could
224 move medio-laterally. Consequently, this configuration provided the tibio-femoral joint with
225 all six DOFs. The patello-femoral joint was modelled with the assumption of a constant length
226 of the patellar tendon, while the three translational DOFs and the spin and tilt (patellar rotation
227 around respectively the anterior-posterior axis and the proximal-distal axis) were solved by the
228 FDK solver. A simple linear torsional spring with spring constant of 100 Nm/rad was included
229 to ensure some stiffness in the patellar tilt direction during deep knee flexion when the patellar
230 ligaments were slack.

231 **4.2.2. Force-dependent kinematics**

232 Knee kinematics were simulated using FDK, an extended inverse dynamics approach, which
233 simultaneously computes ligament forces and secondary joint motions [10]. This methodology
234 relies on an assumption of quasi-static force equilibrium in the secondary joint kinematics at
235 each time step during the analysis, eliminating the need for time integration. This assumption
236 of static equilibrium only applies to the FDK directions and the full dynamics in all other DOFs
237 are taken into account. This modelling approach is implemented into the AnyBody Modeling
238 System (AnyBody Technology, A/S, Aalborg, Denmark).

239 **4.3. Data analysis**

240 **4.3.1. Sensitivity study**

241 A sensitivity analysis was performed to investigate the influence of the tibio-femoral model
242 parameters on the output. The insertion points of three ligament line segments (MCLprox,
243 MCLdist and LCL) as well as the patellar tendon were moved from their reference position.
244 Since the attachment of these structures is known to lay on the bone surface, the attachments
245 were varied in a plane tangent to the bone surface.

246 From a study investigating the precision in locating landmarks on CT scans, an estimate of the
247 appropriate variability was made [14]. In the study, an intra-variability of around 1 mm and the
248 inter-variability was 3.5 mm or less was reported. Based on these results, a variation of 3.5 mm
249 was first chosen, representing a range of 7 mm.

250 Consequently, all ligaments insertions were varied from -3.5 mm to +3.5 mm in the anterior-
251 posterior and proximal-distal direction. The insertions of the patellar tendon were varied from
252 -3.5 mm to +3.5 mm in the medial-lateral and anterior-posterior direction. When one of the
253 insertion locations was changed, the reference ligament length was recalculated and updated
254 prior to the simulation.

255 In addition, the stiffness and reference strain of the three ligament line segments were varied,
256 each from +3.5% to -3.5% of their reference value. A total of 45 configurations were analysed
257 and the overview of these simulations can be found in Table 2.

258 **4.3.1. Metrics**

259 The tibio-femoral rotations were derived using the Grood and Suntay protocol and the
260 translations were reported in the tibial reference frame [20]. Positive values were assigned to
261 medial, anterior and proximal translations and to valgus and external tibial rotations. Each of
262 these trials show the downwards motion of a squat.

263 The differences between the experimental and simulation results were quantified using the
264 Root-Mean-Square-Error (RMSE) and the Pearson correlation coefficient with ρ categorized as
265 $\rho \leq 0.35$, $0.35 < \rho \leq 0.67$, $0.67 < \rho \leq 0.9$, $0.9 < \rho$ to be weak, moderate, strong or excellent
266 correlations[21,22]

267 **5. Results**

268 The computed tibio-femoral translations (Figure 3) and rotations (Figure 4) showed a good
269 agreement, predicting the proximal-distal, medial-lateral, anterior-posterior, varus-valgus,
270 internal-external motions with an average RMSE of respectively 1.0 mm, 1.2 mm, 2.7 mm, 0.7°
271 and 2.3° . The average Pearson correlation coefficient for the aforementioned motions was 1.00,
272 0.38, 0.85, 0.93 and 0.95, showing strong or excellent correlations except for the medial-lateral
273 motion. This lower correlation is caused by the low order of magnitude of this motion. An
274 overview of the kinematic RMSE and Pearson correlation coefficient for all trials for each
275 cadaver can be found in Table 3.

276 Additionally, tibio-femoral motion can be more intuitively analysed when the 3D motion is
277 projected onto a two-dimensional (2D) plane. Figure 5 shows the projected tibio-femoral
278 kinematics during squat. Because of the clinical importance of rotational movement, the
279 projection plane of choice was the tibial horizontal plane. This plane is defined as the plane
280 perpendicular to the tibial mechanical axis and comprises the line connecting the tibial condyle
281 centres. The projections of the centres of the medial and lateral femoral condyles onto the tibial
282 horizontal plane were presented for different flexion angles, namely 40° , 60° , 80° and 100° .

283 An overview of the ligament length change RMSE and Pearson correlation coefficient for all
284 trials for each specimen can be found in Table 4. The lateral extensometer length change was
285 compared to the model LCL length change and the medial extensometer length change was
286 compared to the model MCLdist length change. The average RMSE was 2.7% for MCLdist and
287 4.0% for LCL and the average Pearson correlation coefficient was 0.96 and 0.74 for MCLdist
288 and LCL respectively. Figure 6 depicts the predicted subject-specific model length changes
289 compared to the kinematic based experimental length changes for all conditions. The average
290 RMSE was 0.9% for MCLdist and 2.5% for LCL and the average Pearson correlation
291 coefficient was 0.99 and 0.98 for MCLdist and LCL respectively.

292 Figure 7 shows the results of the sensitivity study for the three specimens for the neutral insert
293 trial. The translations were the least sensitive to changes in model parameters. The largest
294 changes can be found in internal-external rotation and ligament length changes, presenting
295 changes up to 3.8° in the maximum internal tibial rotation at the end of the simulation, and up
296 to 6.4% in the absolute ligament length change at the end of the simulation. The perturbed
297 simulations of specimen 2 failed to solve if MCL was less strained, hence we removed these
298 failed output resulting in a smaller shaded area for MCL.

299 **6. Discussion**

300 The motivation of this work was to develop a computational efficient subject-specific model
301 that can predict the relative impact of different implant configurations on kinematics and
302 ligament length change patterns. A validation was performed using *in vitro* kinematics and
303 ligament length changes of different component alignments for three different subjects.

304 The results showed that the kinematics can accurately be predicted, showing an average RMSE
305 of less than 2.7 mm and 2.3° for translations and rotations. The largest RMSE was for anterior-
306 posterior translation. The model consistently underestimated the anterior position of the femur
307 with respect to the tibia during the beginning of the squat, indicating that some anterior-
308 posterior stiffness is missing. In reality, the knee joint is surrounded by the joint capsule
309 membrane, which is lacking in the model. Overall, the kinematics showed an excellent
310 correlation and small RMSE for the three subjects during the three different alignment
311 conditions. The motions are comparable in trend and in magnitude with the results of Baldwin
312 et al., who validated a finite element (FE) knee model with a posterior-stabilised implant for
313 three cadaveric knees inside a mechanical rig [23]. The ligament parameters and attachment
314 sites were optimised by minimising differences between model-predicted and experimental
315 kinematics. They noted average RMSE of less than 1.8 mm and 2.2° for translations and
316 rotations respectively. Without ligament parameter optimisation, our model achieved similar

317 results. Moreover, the predicted kinematics after component malrotation showed comparable
318 RMSE.

319 To evaluate the differences caused by malalignment, the different rows for one specimen can
320 be compared in Figure 5. Valgus malalignment resulted in a more externally rotated starting
321 position of the tibia, whereas varus malalignment caused a slightly more internally rotated tibia
322 compared to the neutral alignment. This presents a direct link to ligament behaviour, since the
323 collateral ligaments are known to be important stabilisers. MCL was more strained in valgus
324 and acts as a restraint to tibial internal rotation, LCL experienced more strain in varus,
325 increasing the restraint to tibial external rotation [24].

326 Next to changes introduced by coronal malalignment, the inter-specimen variability influenced
327 the kinematics as well. Even though the contact geometry was identical for all specimens,
328 different kinematic behaviour between the specimens can be seen, in particular with respect to
329 the amount of anterior-posterior translation. Nevertheless, the model was able to closely match
330 the experimental kinematics for each specimen. All specimens showed posterior femoral
331 rollback laterally, abnormal anterior femoral translation medially was present for Specimen 1.
332 Similar inter-specimen variability of kinematics after TKA was also seen *in vivo* [23].
333 Abnormal anterior motion was mostly attributed to lack of PCL and unbalanced collateral
334 ligaments [26]. This explanation seems plausible, since anterior translation was mostly present
335 for varus malalignment of Specimen 1, where 5° of malalignment was introduced as opposed to
336 the 3° of malalignment in Specimen 2 and 3. During varus malrotation, MCL was more slack,
337 resulting in more instability.

338 From the sensitivity study, it is clear that the ligament length change is sensitive to the model
339 parameters. However, the trend of ligament behaviour as a function of implant alignment can
340 be captured by the model. When comparing the extensometer length changes to the model, an
341 excellent average correlation of 0.96 and RMSE of 2.7% was seen for MCL, while LCL had a

342 strong average correlation of 0.74 and an RMSE of 4.0%. Extensometer length changes are
343 local length changes measured at the mid-region of the ligament, whereas the reported model
344 length changes show average length changes between the insertion points. Hence, additional to
345 the local extensometer length changes, the kinematic based ligament length changes were
346 reported, since experimental ligament length changes are often described using the length
347 between the ligament insertions during the reproduced motion [27]. In our study, these
348 kinematic based length changes showed a strong to excellent correlation and the average RMSE
349 is below 2.5% for all ligament segments. The local extensometer and kinematic based
350 experimental length changes agreed well for MCL, while showing larger deviations for LCL,
351 indicating that the simple ligament model cannot fully represent the variable behaviour of the
352 LCL.

353 This study investigated the relative behaviour of ligament length changes when varying implant
354 alignment. When introducing the different configurations for the tibial insert, the model and
355 kinematic based experimental strains showed an analogous behaviour. This behaviour is
356 consistent with the results of Delport et al. [28]. They reported that both for the neutral aligned
357 as for the varus or valgus configurations, MCL as well as LCL remained isometric in the
358 beginning of the squat and then started to relax. In addition, the relative relationship between
359 the varus, neutral and valgus alignment corresponds well to our results, resulting in more MCL
360 strain and less LCL strain for valgus malalignment and the other way around for varus
361 malalignment.

362 The use of mechanical knee simulators in validation studies is a cost-effective and controlled
363 method to mimic real-life conditions. However, this set-up differs from the actual physiologic
364 loading condition, for instance keeping the hip fixed over the ankle and the constant hamstrings
365 load. Despite this artificial representation, the knee motions agree well with *in vivo* motions,
366 supporting the use of such rigs as an intermediate step towards clinical application. Two studies

367 of Victor et al. looked at knee motions, one in a mechanical rig [14] and one in real patients
368 [29]. The *in vitro* study with cadaver knees in a mechanical rig showed mean ranges of motion
369 for tibial rotation and for posterior translation of the medial and lateral femoral condyle of
370 respectively 9.7°, 12.9 mm and 16.3 mm for a PS implant [14]. In the second study, *in vivo*
371 kinematics were measured in TKA patients during deep knee bend with the help of dynamic
372 fluoroscopy [29]. The average range of the aforementioned motions was 10.8°, 14 mm and 23
373 mm.

374 The results of the current study need to be seen within the light of the following limitations.
375 The same implant type was used in all three specimens, which meant sacrificing the cruciate
376 ligaments. Cruciate-retaining implants were not tested. Furthermore, the reported extensometer
377 values show only the ligament length changes at the location where the extensometer is sutured.
378 However, ligaments show different length change behaviour at different locations. Ligament
379 model parameters were based on values from literature to demonstrate the generic workflow.
380 However, it is known that ligament zero-load lengths are sensitive parameters in computational
381 models but difficult to measure [30–32]. Other studies often optimize these zero-load lengths
382 until the rotational knee behaviour matches the experimental data [33]. Finally, only coronal
383 implant position variation is modelled here. In future work, we plan to investigate other implant
384 configuration such as joint line variation.

385 In summary, this work presented a model-based and experimental evaluation of the prediction
386 of knee kinematics and ligament length changes for three different subjects following TKA.
387 Malalignment was introduced and the associated changes in knee kinematic and ligament length
388 change patterns could be predicted well by the model. Despite the identical implant geometry,
389 inter-specimen differences were both experimentally observed and predicted by the subject-
390 specific model. This validation study is a first, necessary step towards the clinical application
391 of musculoskeletal models. Model credibility to predict component malalignment was assured

392 in this work and the current results support the potential of subject-specific musculoskeletal
393 modelling to aid surgeons in deciding the optimal implant configuration for a patient.

394 **Conflict of interest**

395 The authors declare that they have no conflicts of interest.

396 **7. Acknowledgments**

397 This work has financial support by the Baekeland scheme of the agency for Innovation by
398 Science and Technology (IWT) under grant number IWT 110554 to V. Vanheule and the
399 Danish Council for Independent Research (DFF) under grant number DFF-4184-00018 to M.
400 S. Andersen.

401

402

403

404

405

406

407

408

409

410

411

412

413 **8. References**

- 414 [1] Griffin FM, Insall JN, Scuderi GR. Accuracy of soft tissue balancing in total knee
415 arthroplasty. *J Arthroplasty* 2000;15:970–3.
416
- 417 [2] Abdel MP. Measured resection versus gap balancing for total knee arthroplasty. *Clin*
418 *Orthop Relat Res* 2014;472:2016–22.
419
- 420 [3] Fregly BJ, Besier TF, Lloyd DG, Delp SL, Banks SA, Pandy MG, et al. Grand challenge
421 competition to predict in vivo knee loads. *J Orthop Res* 2012;30:503–13.
422
- 423 [4] Amiri S, Cooke D, Kim IY, Wyss U. Mechanics of the passive knee joint. Part 2:
424 interaction between the ligaments and the articular surfaces in guiding the joint motion.
425 *Proc Inst Mech Eng Part H J Eng Med* 2007;221:821–32.
426
- 427 [5] Wilson DR, Feikes JD, O'Connor JJ. Ligaments and articular contact guide passive knee
428 flexion. *J Biomech* 1998;31:1127–36.
429
- 430 [6] Hast MW, Piazza SJ. Dual-joint modeling for estimation of total knee replacement
431 contact forces during locomotion. *J Biomech Eng* 2013;135:021013.
432
- 433 [7] Thelen DG, Won Choi K, Schmitz AM. Co-Simulation of Neuromuscular Dynamics and
434 Knee Mechanics During Human Walking. *J Biomech Eng* 2014;136:021033.
435
- 436 [8] Guess TM, Stylianou AP, Kia M. Concurrent prediction of muscle and tibiofemoral
437 contact forces during treadmill gait. *J Biomech Eng* 2014;136:021032.
438
- 439 [9] Andersen MS, Damsgaard M, Rasmussen J. Force-dependent kinematics : a new analysis
440 method for non-conforming joints. 13th Bienn. Int. Symp. Comput. Simul. Biomech.,
441 2011.
442
- 443 [10] Marra MA, Vanheule V, Rasmussen J, Verdonschot NJJ, Andersen MS. A Subject-
444 Specific Musculoskeletal Modeling Framework to Predict in Vivo Mechanics of Total
445 Knee Arthroplasty. *J Biomech Eng* 2014;137:020904.
446
- 447 [11] Thompson JA, Hast MW, Granger JF, Piazza SJ, Siston RA. Biomechanical effects of
448 total knee arthroplasty component malrotation: A computational simulation. *J Orthop*
449 *Res* 2011;29:969–75.
450
- 451 [12] Chen Z, Wang L, Liu Y, He J, Lian Q, Li D, et al. Effect of component mal-rotation on
452 knee loading in total knee arthroplasty using multi-body dynamics modeling under a
453 simulated walking gait. *J Orthop Res* 2015;33:1287–96.
454

- 455 [13] Werner FW, Ayers DC, Maletsky LP, Rullkoetter PJ. The effect of valgus/varus
456 malalignment on load distribution in total knee replacements. *J Biomech* 2005;38:349–
457 55.
458
- 459 [14] Victor J, Bellemans J. A comparative study on the biomechanics of the native human
460 knee joint and total knee arthroplasty. *Dep Orthop Fac Med* 2009;PhD.
461
- 462 [15] Delpont H, Labey L, De Corte R, Innocenti B, Vander Sloten J, Bellemans J. Collateral
463 ligament strains during knee joint laxity evaluation before and after TKA. *Clin Biomech*
464 2013;28:777–82.
465
- 466 [16] Zavatsky AB. A kinematic-freedom analysis of a flexed-knee-stance testing rig. *J*
467 *Biomech* 1997;30:277–80.
468
- 469 [17] Blankevoort L, Huiskes R. Ligament-bone interaction in a three-dimensional model of
470 the knee. *J Biomech Eng* 1991;113:263–9.
471
- 472 [18] Butler DL, Kay MD, Stouffer DC. Comparison of material properties in fascicle-bone
473 units from human patellar tendon and knee ligaments. *J Biomech* 1986;19:425–32.
474
- 475 [19] Amis AA, Firer P, Mountney J, Senavongse W, Thomas NP. The anatomy and
476 reconstruction of the medial patellofemoral ligament. *Knee* 2003;10:215–20.
477
- 478 [20] Grood ES, Suntay WJ. A Joint Coordinate System for the Clinical Description of Three-
479 Dimensional Motions: Application to the Knee. *J Biomech Eng* 1983;105:136–44.
480
- 481 [21] Taylor R. Interpretation of the Correlation Coefficient: A Basic Review. *J Diagnostic*
482 *Med Sonogr* 1990;6 :35–9.
483
- 484 [22] Fluit R, Andersen MS, Kolk S, Verdonshot N, Koopman HFJM. Prediction of ground
485 reaction forces and moments during various activities of daily living. *J Biomech*
486 2014;47:2321–9.
487
- 488 [23] Baldwin MA, Clary CW, Fitzpatrick CK, Deacy JS, Maletsky LP, Rullkoetter PJ.
489 Dynamic finite element knee simulation for evaluation of knee replacement mechanics.
490 *J Biomech* 2012;45:474–83.
491
- 492 [24] Athwal KK, Hunt NC, Davies AJ, Deehan DJ, Amis A a. Clinical biomechanics of
493 instability related to total knee arthroplasty. *Clin Biomech* 2014;29:119–28.
494
- 495 [25] Dennis D a, Komistek RD, Colwell CE, Ranawat CS, Scott RD, Thornhill TS, et al. In
496 Vivo Anteroposterior Femorotibial Translation of Total Knee Arthroplasty: A

- 497 Multicenter Analysis. *Clin Orthop Relat Res* 1998;353:47–57.
498
- 499 [26] Cromie MJ, Siston RA, Giori NJ, Delp SL. Posterior cruciate ligament removal
500 contributes to abnormal knee motion during posterior stabilized total knee arthroplasty.
501 *J Orthop Res* 2008;26:1494–9.
502
- 503 [27] Park SE, DeFrate LE, Suggs JF, Gill TJ, Rubash HE, Li G. Erratum to “The change in
504 length of the medial and lateral collateral ligaments during in vivo knee flexion”. *Knee*
505 2006;13:77–82.
506
- 507 [28] Delport H, Labey L, Innocenti B, De Corte R, Vander Sloten J, Bellemans J. Restoration
508 of constitutional alignment in TKA leads to more physiological strains in the collateral
509 ligaments. *Knee Surgery, Sport Traumatol Arthrosc* 2015;23:2159–69.
510
- 511 [29] Victor J, Mueller JKP, Komistek RD, Sharma A, Nadaud MC, Bellemans J. In Vivo
512 Kinematics after a Cruciate-substituting TKA. *Clin Orthop Relat Res* 2010;468:807–14.
513
- 514 [30] Baldwin MA, Laz PJ, Stowe JQ, Rullkoetter PJ. Efficient probabilistic representation of
515 tibiofemoral soft tissue constraint. *Comput Methods Biomech Biomed Engin*
516 2009;12:651–9.
517
- 518 [31] H. Bloemker K. Computational Knee Ligament Modeling Using Experimentally
519 Determined Zero-Load Lengths. *Open Biomed Eng J* 2012;6:33–41.
520
- 521 [32] Beillas P, Lee SW, Tashman S, Yang KH. Sensitivity of the tibio-femoral response to
522 finite element modeling parameters. *Comput Methods Biomech Biomed Engin*
523 2007;10:209–21.
524
- 525 [33] Pandy MG, Sasaki K, Kim S. A Three-Dimensional Musculoskeletal Model of the
526 Human Knee Joint. Part 1: Theoretical Construction. *Comput Methods Biomech Biomed*
527 *Engin* 1997;1:87–108.
528
- 529

9. Tables

Table 1: Reference strain (ϵ_r) and stiffness (k) values adapted from Blankevoort and Huiskes [17]. The literature values were slightly adapted since our model has two MCL bundles and one LCL bundle while their model has three bundles for both MCL and LCL. The stiffness was redistributed according to the number of bundles, MCL reference strain could be copied and the LCL reference strain was copied such that the bundle was tensioned in full extension. Both MPFL and LEPL consisted of three bundles and the reported parameter values were assigned to each bundle.

	MCL	LCL	MPFL	LEPL
ϵ_r	0.04	0.08	0.08	0.06
k (N)	4125	6000	2000	1000

Table 2: Summary of the different configurations of the sensitivity study. For each configuration, only one model parameter was perturbed while all other model parameters were kept constant.

Component	Measure	Low value	Initial value	High value
LCL tibia	Ant-pos	-3.5 mm	reference	+3.5 mm
	Prox-dis	-3.5 mm	reference	+3.5 mm
LCL femur	Ant-pos	-3.5 mm	reference	+3.5 mm
	Prox-dis	-3.5 mm	reference	+3.5 mm
MCLprox tibia	Ant-pos	-3.5 mm	reference	+3.5 mm
	Prox-dis	-3.5 mm	reference	+3.5 mm
MCLprox femur	Ant-pos	-3.5 mm	reference	+3.5 mm
	Prox-dis	-3.5 mm	reference	+3.5 mm
MCLdist tibia	Ant-pos	-3.5 mm	reference	+3.5 mm
	Prox-dis	-3.5 mm	reference	+3.5 mm
MCLdist femur	Ant-pos	-3.5 mm	reference	+3.5 mm
	Prox-dis	-3.5 mm	reference	+3.5 mm
Patellar tendon tibia	Med-lat	-3.5 mm	reference	+3.5 mm
	Prox-dis	-3.5 mm	reference	+3.5 mm
Patellar tendon patella	Med-lat	-3.5 mm	reference	+3.5 mm
	Prox-dis	-3.5 mm	reference	+3.5 mm
LCL	k	5790 N	6000 N	6210 N
	ϵ_r	0.045%	0.08%	0.115%
MCLprox	k	3980N	4125 N	4270 N
	ϵ_r	0.005%	0.04%	0.075%
MCLdist	k	3980N	4125 N	4270 N
	ϵ_r	0.005%	0.04%	0.075%

Table 3: Comparison of measured and computed kinematics using RMSE and Pearson correlation coefficient ρ . Proximal-distal (PD), medial-lateral (ML), anterior-posterior (AP), varus-valgus (VV) and internal-external (IE) motions are shown.

	RMSE					ρ				
	PD	ML	AP	VV	IE	PD	ML	AP	VV	IE
	(mm)	(mm)	(mm)	(°)	(°)					
Specimen 1										
Neutral	1.34	1.50	2.43	0.67	2.00	1.00	0.40	0.69	0.89	0.94
Varus	1.53	1.16	2.26	0.61	1.97	1.00	0.79	0.66	0.79	0.99
Valgus	0.89	2.19	2.58	0.41	2.91	1.00	-0.08	0.75	0.97	0.94
Specimen 2										
Neutral	0.47	0.89	2.95	0.80	2.65	1.00	0.00	0.91	0.93	0.92
Varus	0.44	0.65	2.18	1.26	3.23	1.00	0.88	0.94	0.99	0.93
Valgus	0.53	0.44	2.41	0.65	2.04	1.00	0.78	0.90	0.86	0.95
Specimen 3										
Neutral	1.38	0.93	3.26	0.45	1.94	0.99	0.43	0.97	1.00	0.97
Varus	1.52	1.82	3.13	0.75	1.58	0.99	-0.16	0.95	1.00	0.97
	1.01	1.20	2.65	0.70	2.29	1.00	0.38	0.85	0.93	0.95
Average	±	±	±	±	±	±	±	±	±	±
	0.45	0.56	0.38	0.25	0.53	0.00	0.39	0.12	0.07	0.02

Table 4: Comparison of experimental and computed ligament length changes using RMSE and Pearson correlation coefficient ρ . Kinematic based length changes (Kin) and extensometer length changes (Ext) are shown.

	RMSE				ρ			
	MCL	MCL	LCL	LCL	MCL	MCL	LCL	LCL
	Ext (%)	Kin (%)	Ext (%)	Kin (%)	Ext	Kin	Ext	Kin
Specimen 1								
Neutral	1.88	0.87	3.45	3.26	0.98	0.99	0.25	0.99
Varus	4.64	1.11	1.99	3.44	0.97	0.99	0.28	0.97
Valgus	2.24	1.09	4.07	1.49	0.96	0.97	0.67	0.95
Specimen 2								
Neutral	2.08	0.44	4.97	1.74	0.99	1.00	0.95	0.97
Varus	2.03	0.76	4.05	2.25	0.94	0.99	0.99	0.98
Valgus	1.87	0.65	3.04	1.39	0.96	0.97	0.98	0.99
Specimen 3								
Neutral	2.83	1.27	5.92	2.73	0.93	0.99	0.87	0.98
Varus	3.95	1.10	4.73	3.82	0.92	0.99	0.92	0.98
Average								
	2.69	0.91	4.03	2.51	0.96	0.99	0.74	0.98
	± 0.98	± 0.26	± 1.14	± 0.88	± 0.02	± 0.01	± 0.29	± 0.01

Figure legends

Figure 1: Illustration of the analytical surfaces that were fitted to the bone and implant geometries as wrapping surfaces. One cylinder was placed medially, allowing the MCLdist to wrap around the medial tibial condyle. Another cylinder was fitted to the femoral implant to prevent the quadriceps muscle from penetrating the implant in deep flexion. Two ellipsoids were introduced to wrap the MPFL and LEPL around the femoral condyles.

Figure 2: Illustration of the simulation of the mechanical rig inside AnyBody. The hip joint has 2 DOFs: vertical translation and flexion-extension. The ankle joint has 4 DOFs: all three rotations and medio-lateral translation. This configuration provides the tibio-femoral joint with all six DOFs. The patello-femoral joint was modelled with the assumption of a constant length for the patellar tendon and the other 5 DOF were solved using FDK.

Figure 3: Comparison of experimental and model tibio-femoral translations of the three specimens. Experimental (marker) and computed (line) proximal-distal (black/circles), medial-lateral (red/crosses) and anterior-posterior (blue/squares) translations are shown. The rows show the results for the different specimens, the columns show the results for the different configurations (varus insert, neutral insert and valgus insert).

Figure 4: Comparison of experimental and model tibio-femoral rotations of the three specimens. Experimental (marker) and computed (line) varus-valgus (black/circles) and internal-external (red/crosses) rotations are shown. The rows show the results for the different specimens, the columns show the results for the different configurations (varus insert, neutral insert and valgus insert).

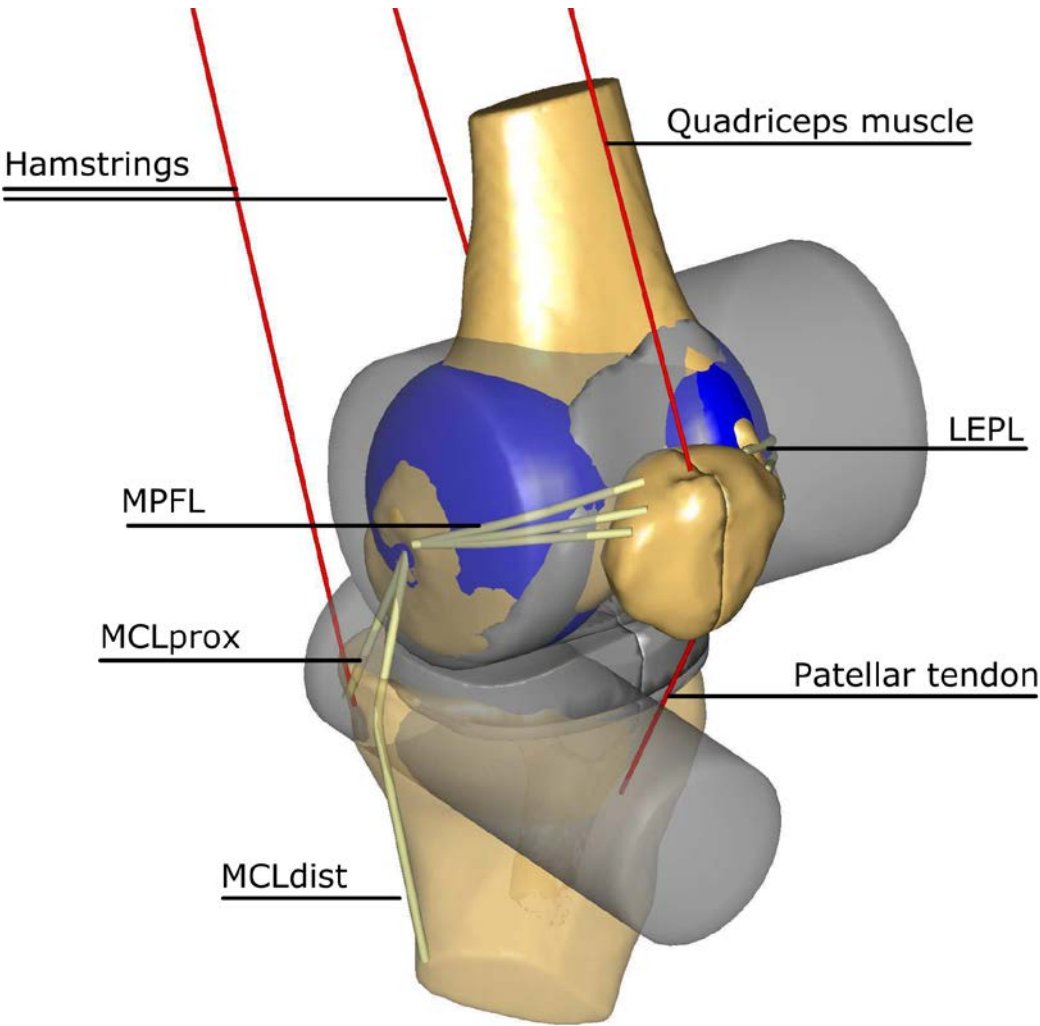
Figure 5: 2D view of experimental (dotted lined) and model kinematics (full line) of the three specimens. The centres of the medial and lateral femoral condy

les are projected onto the tibial horizontal plane for different flexion angles (40°, 60°, 80° and 100°). The rows show the results for the different specimens, the columns show the results for the different configurations (varus insert, neutral insert and valgus insert). The top view of each specimen's left knee is depicted, with the anterior side pointing upwards.

Figure 6: Comparison of kinematic based experimental and model ligament length changes of the three specimens. Experimental (marker) and computed (line) MCLdist (black/circles) and LCL (red/crosses) strains are shown. The rows show the results for the different specimens, the columns show the results for the different configurations (varus insert, neutral insert and valgus insert).

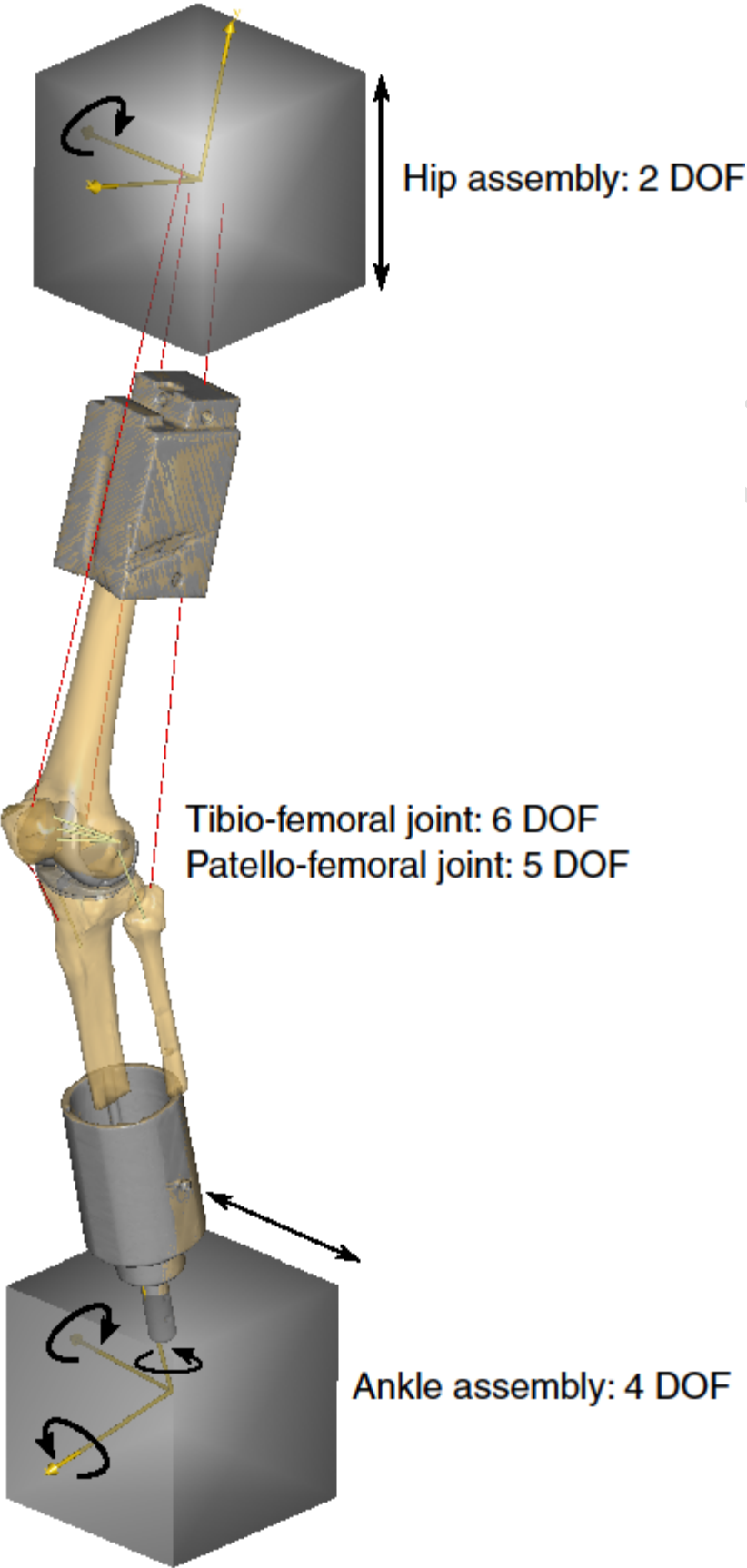
Figure 7: The different output curves of the sensitivity analysis are shown as a shaded area on the figures. The first column shows translations, the second column rotations and the third and fourth column ligament length changes for the neutral configuration of each specimen (rows). The experimental measured data is shown in dotted line and the simulation with reference values in full line. For the translations, proximal-distal (red), medial-lateral (blue) and anterior-posterior (green) is shown. For the rotations, varus-valgus (red) and internal-external (blue) is depicted.

Figure 1



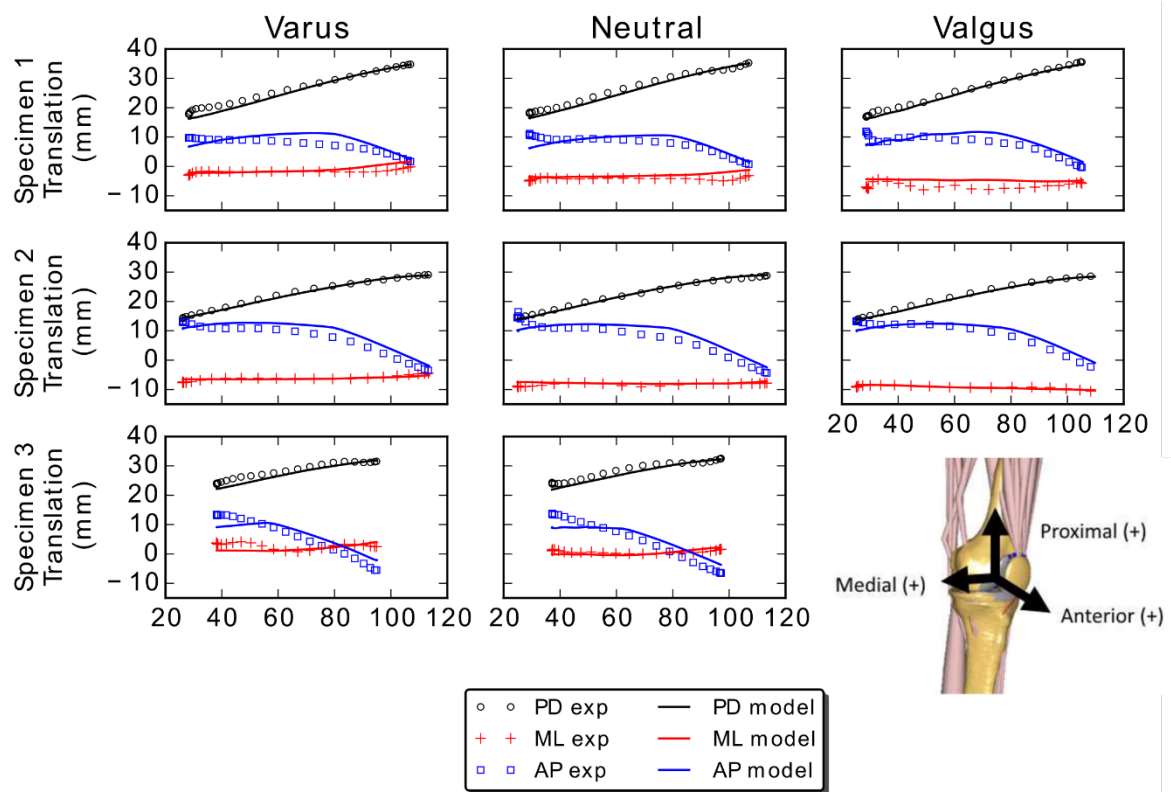
Accepted

Figure 2



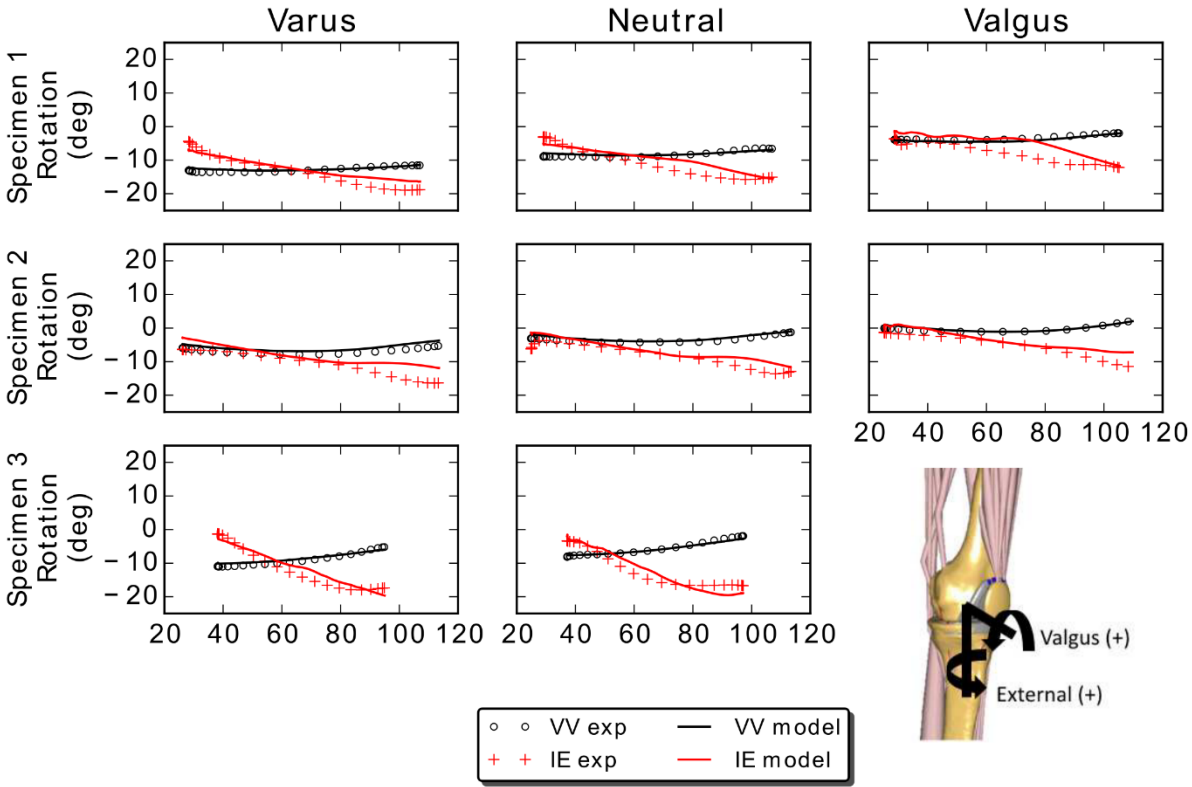
cript

Figure 3



Accepted manuscript

Figure 4



Accepted manuscript

Figure 5

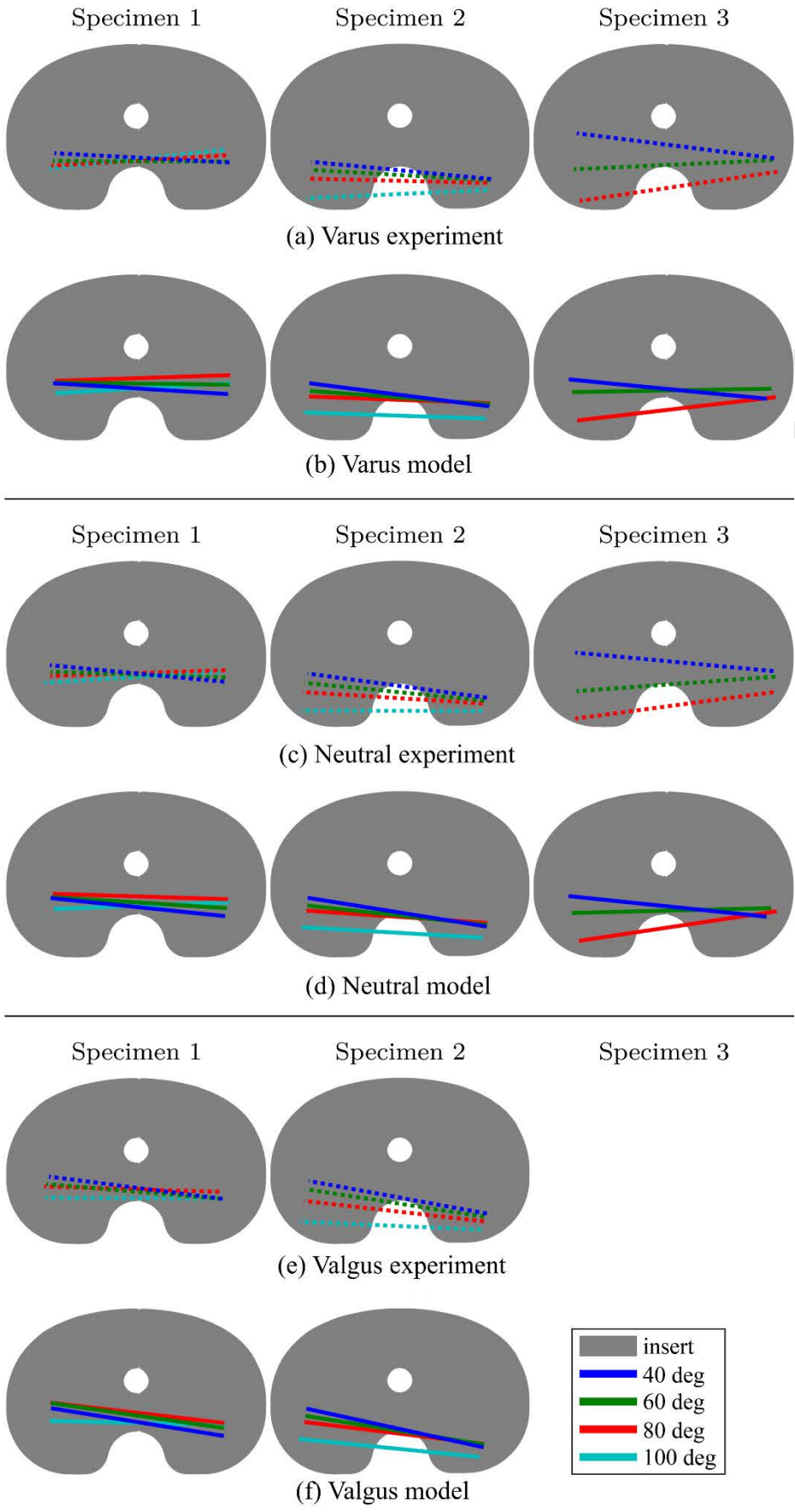
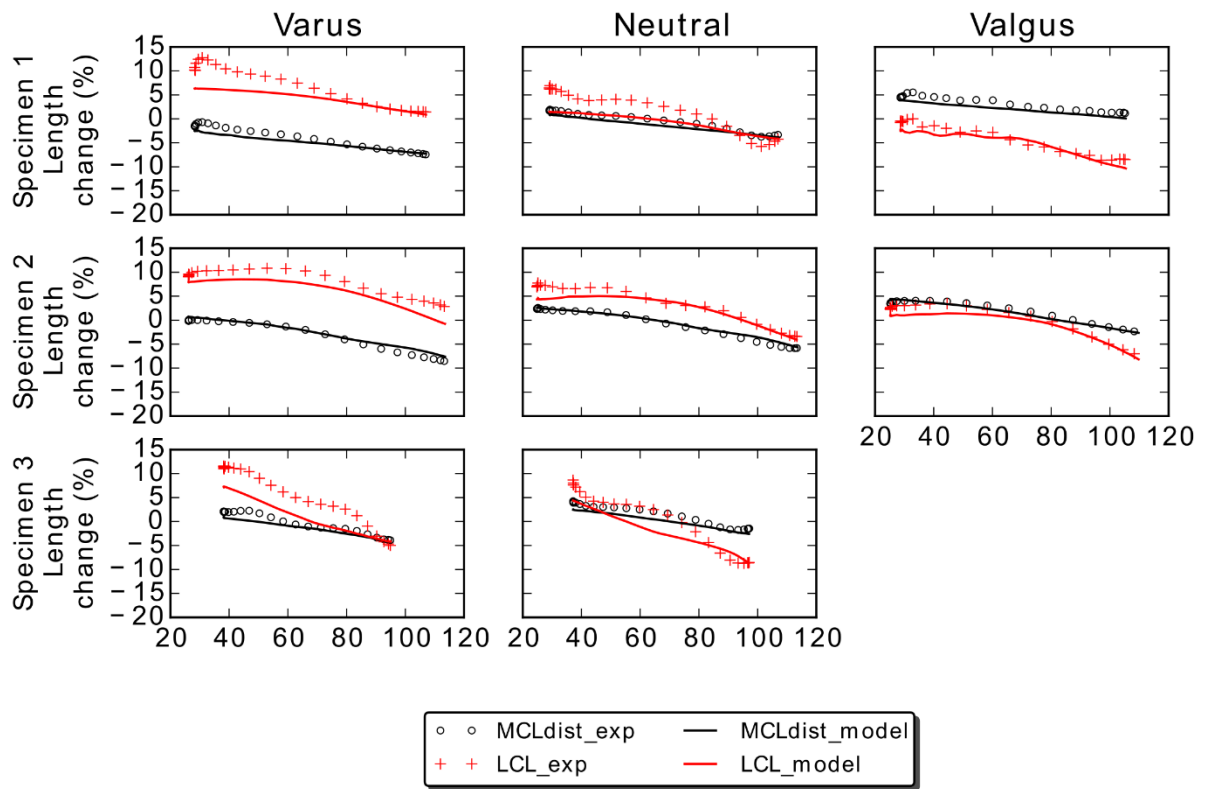


Figure 6



Accepted manuscript

Figure 7

